UNIVERSITY OF CALIFORNIA, SAN DIEGO

A Shadow Histogram Algorithm to Determine Clear Sky Indices for Sky Imager Short Term Advective Solar forecasting

A Thesis submitted in partial satisfaction of the requirements
for the degree Master of Science

in

Engineering Sciences (Mechanical Engineering)

by

Nishank Mihir Sheth

Committee in charge:

Professor Jan Kleissl, Chair
Professor Renkun Chen
Professor Lynn Russell

2016

The Thesis of Nishank Mihir Sheth is approved and acceptable in quality and form for publication on microfilm and electronically:

_____

_____

_____

Chair

University of California, San Diego

2016

TABLE OF CONTENTS

LIST OF FIGURES

LIST OF TABLES

ACKNOWLEDGMENTS

I would like to express my gratitude for Professor Jan Kleissl, who, as my faculty adviser guided me from the very first day. His prompt replies, calm personality and ever so helpful attitude towards students is the reason that I was able to feel comfortable at every step that I took at UCSD. I am very grateful to have had the opportunity to work with him and his bright group which truly taught me more than just academics.

Keenan Murray helped me throughout my journey at every juncture. Hence I would like to thank him, for injecting zeal and motivation into me when I needed it and encouraging me to perform better. His guidance on programming as well as basic concepts and background of sky imagers helped me complete my project.

I am also very thankful to other members of the team; Zack Pecenak for setting me up with the required software, and Ben Kurtz for his valuable feedback on every aspect of my project. Prathamesh has always been a friend as well as a colleague that gave his inputs, feedback and support when I needed it.

Lastly, I would like to express my gratitude for my parents who have constantly encouraged and inspired me at every stage in life; and my brother who set an example for me to work hard as a student and a professional.

Chapters 1, 3, 4 and 5, in part, are currently being prepared for submission for publication of the material. Sheth, Nishank; Murray, Keenan; Kurtz, Ben; Kleissl, Jan. The thesis author was the primary investigator and author for this material.

ABSTRACT OF THE THESIS

A Shadow Histogram Algorithm to Determine Clear Sky Indices for Sky Imager Short Term Advective Solar forecasting

by

Nishank Mihir Sheth

Master of Science in Engineering Science (Mechanical Engineering)

University of California, San Diego, 2016

Professor Jan Kleissl, Chair

Sky imagers are used for short-term forecasting of solar irradiance, which can be used to counter ramp events caused by larger clouds or extensive changes in cloud cover. Sky imager forecast algorithms usually detect cloud classes in the image. However, the assignment of cloud optical depth or surface Global Horizontal Irradiance (GHI) to cloud classes remains a challenge. One method to connect GHI to cloud classes involves the use of a histogram of recently measured clear sky indices to assign a clear sky index/GHI to each cloud class. While this method improves upon choosing static GHI values for each cloud class, this paper presents a modification which improves the histogram method. Considering data

from a significantly shorter time period than the existing method emphasizes more recent cloud conditions. Individual histograms for each cloud class self-consistent with modeled cloud coverage from the sky imager are used to analyze the data instead of a single histogram. The new algorithm gave a 39% reduction in root mean square error against the existing algorithm when tested over a month.

Keywords: solar, forecast, GHI, algorithm, whole sky imager

1. INTRODUCTION

Sky imagers take images of the sky at regular short intervals which are processed to determine cloud cover, optical depth (whether the cloud is thin or thick), and mean cloud field velocity. Ground based imagers have been employed for forecasting cloud cover for forecast horizons of 30 seconds, 1 minute, and 5 minutes with mean matching error less than 8.7%, 13% and 30% respectively [1]. The positions of the cloud are then forecasted by the sky imager using a cloud advection algorithm up to various forecast horizons. An error metrics then analyzes the performance of the sky imager for every time step.

Sky imagers use a binary or trinary cloud decision algorithms to provide short term forecasts of solar irradiance. Cloud decision algorithms detect clouds in the sky by assigning each image pixel a cloud class based on the ratio of the red channel of the RGB image to its blue channel, also called red-blue ratio or RBR [2]. A binary cloud decision algorithm can detect either cloud or clear sky and could reduce accuracy and make a GHI forecast more discrete.

Sky imager groups have used different approaches to estimate solar irradiance. [3] uses five cloud classes and each pixel of the image is assigned a weight calculated using topo-centric elevation and azimuth angle. Assuming a fixed brightness coefficient for each cloud class, and using linear regression, GHI and Direct Normal Insolation (DNI) are estimated. [4] uses a binary cloud decision algorithm followed by the formation of a histogram with measured ground data to

estimate GHI, similar to that of the sky imager used at UCSD. The formation of a single histogram with measured ground data from a particular time period to estimate GHI has shown moderately good results irrespective of a binary or trinary cloud decision algorithm (trinary has shown better results owing to the increase in cloud classes, reducing the discreteness in the GHI estimation). Yet, common drawbacks are faced. The UCSD sky imager (USI) uses a trinary cloud decision which detects thick cloud, thin cloud, or clear sky. An existing GHI algorithm uses readings from the past 90 minutes acquired from 6 Li-200 pyranometers (Fig. 1) which provide 1 second GHI data and are present at UCSD to create a histogram which analyzes measured power data converted to a clear sky index '*kt*.' *kt* is the ratio of global horizontal irradiance and a reference clear sky irradiance [5].

Figure 1. Map of UCSD footprint showing the locations of pyranometers and the location of USI at UCSD. The labels marked in yellow represent pyranometres that came online after November 2013 and thus did not contribute to the data represented in this thesis.

Three peaks are detected in this histogram from acceptable bounds assigned to each cloud class. These represent the modal transmissivities of clear sky, thin clouds, and thick clouds respectively. If a peak cannot be detected, default values are used. This provides a quantitative estimate of solar energy, a step forward from the initial forecasts of just cloud decision, but does not adapt well to constantly changing cloud conditions due to its large lookback period of 90 minutes. The method also forces us to select a *kt* value for a particular cloud class from a particular bound assigned to that cloud class within the histogram. This is not always the case; for instance, a thin cloud *kt* might have a similar value to a thick cloud *kt* on another day. Cloud enhancements occur near thin clouds but have a *kt* value of more than 1, which is another example supporting this argument [6]. The existing algorithm in that case assigns default values which reduces accuracy. An algorithm was developed where the lookback period was reduced and differed for every forecast based on the quantity of data acquired in that step. It did not constrain the value of the *kt* index with a particular range. This significantly aided it to adapt better to sudden cloud formation or dissipation and give a result that depends on more recent occurrences in the sky. This thesis is aimed at describing and evaluating the ‘Shadow Histogram’ algorithm intended at reducing error in GHI forecasts.

Chapter 1 in part, is currently being prepared for submission for publication of the material. Sheth, Nishank; Murray, Keenan; Kurtz, Ben; Kleissl, Jan. The thesis author was the primary investigator and author for this material.

2. THEORY

Solar power forecasting is a knowledge of the Sun's path, the condition of the atmosphere and the sky, the scattering processes, and the characteristics of the power plant which uses solar energy to generate electric power. Forecasting is significant to the efficient use, management of the electric grid and for solar energy trading.

174,000 terawatts (TW) of incoming solar radiation, also called insolation is received at the Earth's surface [7]. 30% reflects back to space while the rest is absorbed by clouds, oceans and land masses. Most of the world's population live in regions where insolation levels reach 3.5-7.0 kWh/m^2 per day. In 2002, the 3,850,000 exajoules (EJ) received in a year was more energy per day than the world used in the entire year [8]. Solar power, or the process of converting solar energy to electricity, has been either directly carried out using photovoltaics (PV), or indirectly using concentrated solar power (CSP).

Photovoltaic (PV) electricity generation is making major inroads in electricity grids worldwide. Growth rates in installed capacities ranging 34% to 82% for OEC countries over the past decade and installed capacities reaching 63.6 GW in the same countries by end of 2011 [9]. 30% of overall power production during clear days in the summer in some European countries comes from PV production.

Variability and uncertainty are major challenges to high penetration rates of PV systems. Output from PV systems varies at every timescale, from seconds to

even years. Short term changes in the conditions of the sky are difficult to predict and hence, regulating and maintaining power are both challenging and costly. Sudden and widespread changes in irradiance, termed as “ramp events,” which are caused by large clouds or widespread changes in cloud cover [10], are of particular interest for research in short term solar irradiance forecasting. Ramp events require ancillary services to ramp up or down to meet the change in electrical supply and maintain power quality. Reduction in the uncertainty of solar generation through accurate solar forecasting reduces solar integration costs.

Solar radiation forecasting has been tackled by two main approaches: physics based numerical weather prediction (NWP), and forecasting that is more directly based on real-time measurements from satellites or ground-based instruments, although the boundaries between these approaches are constantly becoming more fluid, and machine learning techniques often synthesize the various approaches [11] [12] [13] [14]. [15] and [16] found that NWP forecasts generally perform better than satellite forecasts at forecast horizons longer than a few hours. The limited resolution and uncertainty in initial conditions makes NWP models presently unable to predict the exact position of clouds and their effect on solar radiation over a specific location. Therefore, better short-term measurement-based forecasts at high spatial and temporal resolutions need to be developed.

Deterministic measurement-based forecasting is typically based on satellite [17] or ground-based sky images. Sky imager approaches had only been applied recently for 15 min DNI [18], 10 min GHI, and AC power forecasting for 48 MW of photovoltaics [19] using the Total Sky Imager (TSI, Yankee Environmental

Systems). A proposed requirement by the Puerto Rico Electric Power Authority on utility-scale photovoltaic (PV) power plants in Puerto Rico limiting both up and down ramp events to 10% of capacity per minute [20] drove the first significant market need for 1–15 min solar power forecasts.

3. METHODOLOGY

The USI and many other sky imagers have used a histogram method to forecast GHI as described earlier. Yet, predicting GHI accurately has remained a challenge even after successfully forecasting cloud decision. The USI uses one such histogram method to estimate GHI, but faces challenges that decrease efficiency. Hence, a new algorithm was developed to modify the histogram method to produce better results and adapt well against conditions that earlier created higher errors.

3.1. Cloud decision

The UCSD short-term forecast algorithm uses a trinary cloud classification: thick cloud, thin cloud, and clear sky, as can be seen in Fig 2., which shows the steps associated to the functioning of the sky imager [5]. The UCSD area had 6 pyranometers in use in 2012. The cloud decision algorithm detects whether a pixel on the image is clear sky, thin cloud, or thick cloud based on the RBR. Due to this detection, the type of cloud class over each of the 6 sensors is known at every timestep.

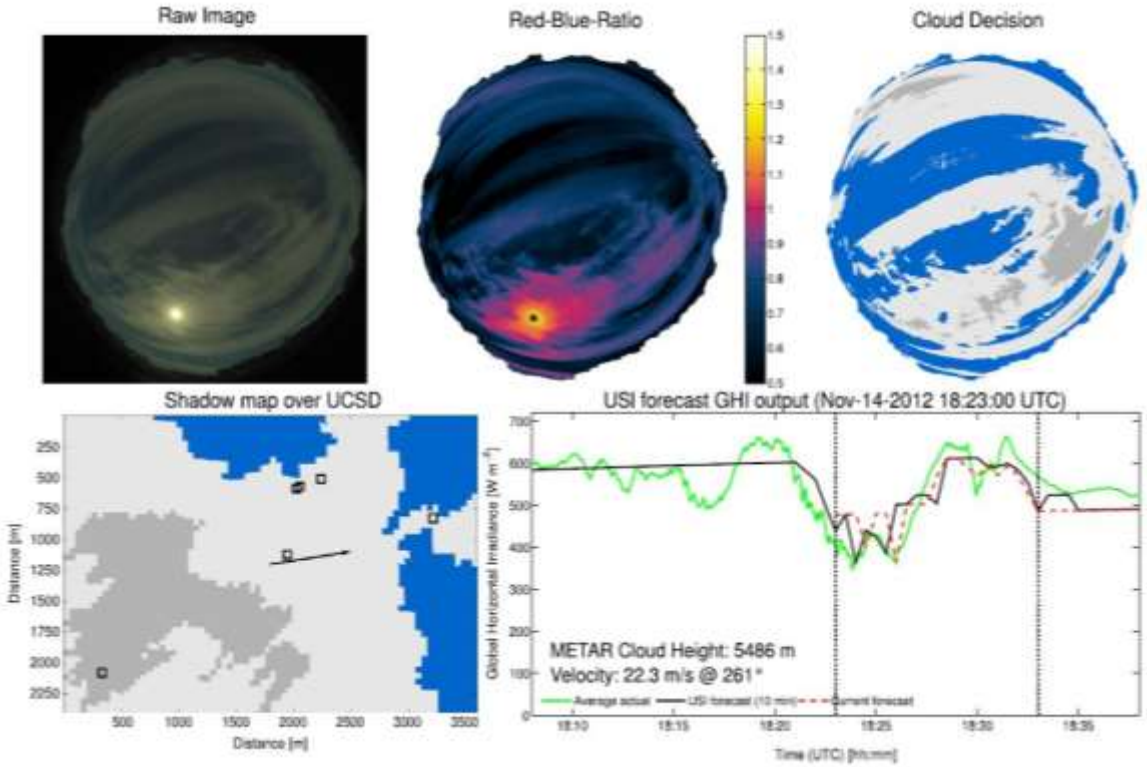

Figure 2. Example of USI forecast output for November 14, 2012, 10:23:00 PST. Top left: raw HDR image, cropped to remove static objects near horizon. Top center: red–blue-ratio image. Top right: cloud decision image (blue: clear sky, light gray: thin cloud, dark gray: thick cloud). Bottom left: shadow map over the UCSD domain, showing predicted cloud shadows from images taken 10 min ago. Ground stations are marked by solid black squares. The cloud field mean velocity vector is indicated by the solid black arrow extending from the center, with magnitude indicating predicted distance traveled in 30 s. Bottom right: USI GHI forecast issued at current time for a 15 min horizon (dashed red), USI GHI forecast time series for constant 10 min forecast horizon (solid black), and corresponding measured GHI (solid green). All measurements and USI forecasts are averaged across all 6 ground stations. The first vertical dashed line indicates forecast issue time, while the second vertical dashed line shows the 10 min forecast horizon (solid black line must equal red dashed line at that point).

The histogram created for a time t_0 for any cloud class *cc*, *hist(cc)* is a set of measured *kt* for that cloud class kt_{cc} from all sensors over a lookback period *l*. A $kt_{s,t}$ measured by any of the 6 UCSD pyranometers *s* at any time *t* is assigned

to a cloud class cc (clear sky cl, thin cloud tn, or thick cloud tk) based on the cloud detection of the USI (UCSD sky imager) over the sensor as

$$hist(cc) = \{kt_{s,t} |\ cc\ (USI, s) = cc\}, t_0 - l \leq t \leq t_0, cc = \{cl, tn, tk\} \qquad (1)$$

The algorithm generates one histogram for each cloud class using these values of *kt* for a lookback period. In order to form histograms with this data, a lookback period is used. A lookback period is the time in minutes that the algorithm goes back to include data for the histograms. The length of the lookback period is extended back in time starting with 5 minutes to fill each cloud class histogram with at least 10 measurements. Increasing this value of minimum measurements increased the length of the lookback period with only minute effects on the results when tested over the month. Therefore, an optimum number was chosen to represent a cloud class with enough data while limiting the length of the lookback period. If the lookback time exceeds 20 minutes, default kt values are chosen. The mode of each histogram, kt_{cc} is used as the *kt* of the respective cloud class. Allowable *kt* values are between 0 and 1.4.

3.2. Forming histograms

Quite often, due to extremely overcast or clear sky conditions, data for particular cloud classes may not be obtained in the past 5 minutes. This leaves the algorithm with no values to forecast if there are occurrences such as sudden cloud formation or dissipation. In order to counter this, the length of the lookback period depends on recent cloud cover, as the algorithm will search further back in time to fill each cloud class histogram with atleast 10 measurements. If the lookback time

exceeds the maximum allowable limit set forth, default values that have been obtained from 8 months of observational data are taken. Default values of *kt* were taken as 0.42 for thick clouds, 0.70 for thin clouds, and 1.05 for clear sky. This usually occurs due to an overcast or clear sky condition for extended periods of time followed by sudden cloud dissipation or formation, respectively.

This ensures that the algorithm always has values for all cloud classes to adapt to suddenly changing cloud conditions, and also significantly reduces lookback period compared to the existing algorithm.

The algorithm generates one histogram for each cloud class using these values of *kt* for a lookback period.

3.3. Forecasting *kt*

The mode of each histogram is used as the *kt* of the respective cloud class. This method permits a cloud class to have a *kt* index anywhere below 1.4 which is considered the maximum allowable *kt*; which is an advantage over the existing method.

As seen in Fig. 3, The existing method is forced to select a *kt* for each cloud class from a predefined range on a single histogram. This may not always be the case. For instance, cloud enhancement occurs near thin cloud but *kt* associated with it is more than 1 (Pecenak, et al. 2016). Sometimes, cloud classes do not have those values of *kt* that the existing algorithm is restricted to assign to them due to the bounds in the histogram.

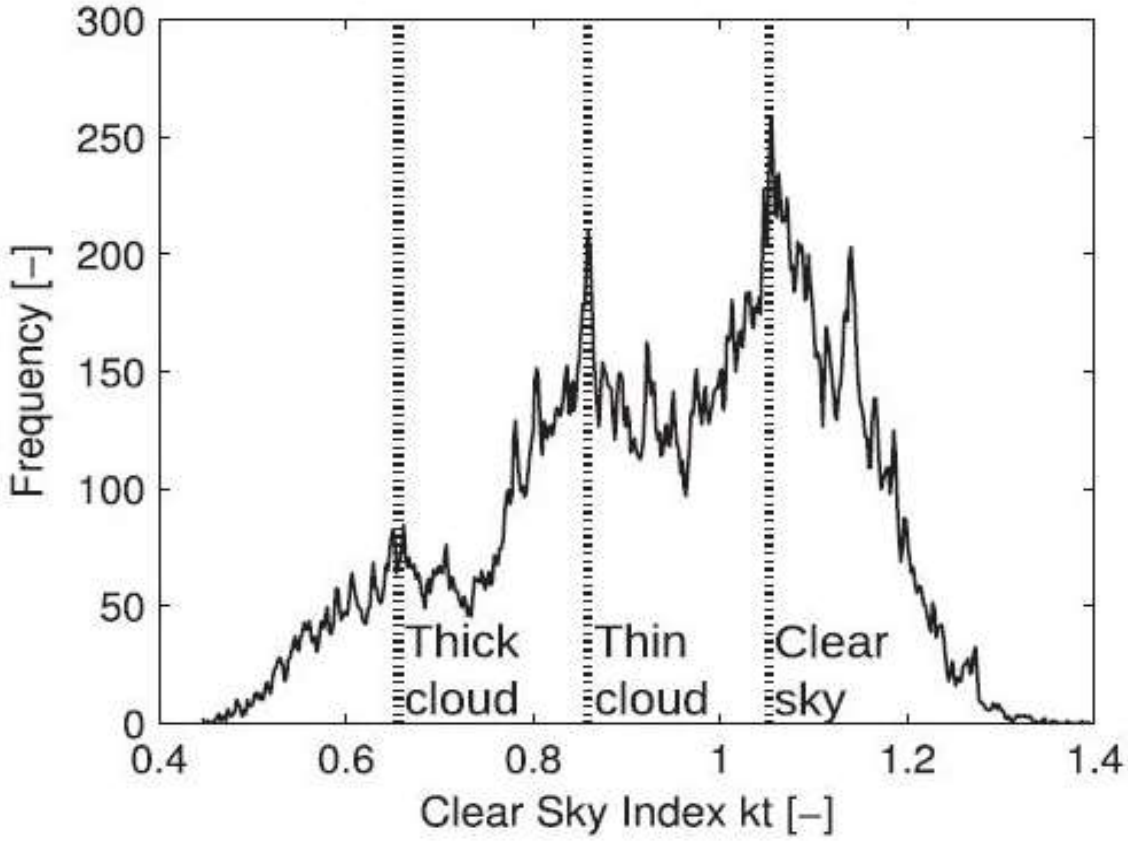

Figure 3. Histogram of measured kt using the existing method for November 14, 2012 10:00:00 PST through 12:00:00 PST, illustrating three distinct peaks representative of thick clouds, thin clouds and clear sky.

The three values of *kt* for the respective cloud classes are assigned to each pixel of the forecasted cloud decision within the footprint depending on whether they are predicted to be covered by clear sky, thin cloud, or thick cloud. The *kt* values ($kt_{forecast}$) for each pixel are then multiplied by Kasten clear sky model GHI ($GHI_{clear\ sky}$) to produce a GHI forecast ($GHI_{forecast}$).

$$GHI_{forecast} = kt_{forecast}\ x\ GHI_{clear\ sky} \quad (2)$$

Plant power output, can be estimated by calculating a weighted-area average *kt* over the entire footprint. The algorithm was evaluated for the month of November 2012 barring 12th November and compared with the existing method. Data for 12th November was not available due to the USI system outage.

Chapter 3 in part, is currently being prepared for submission for publication of the material. Sheth, Nishank; Murray, Keenan; Kurtz, Ben; Kleissl, Jan. The thesis author was the primary investigator and author for this material.

4. RESULTS AND DISCUSSIONS

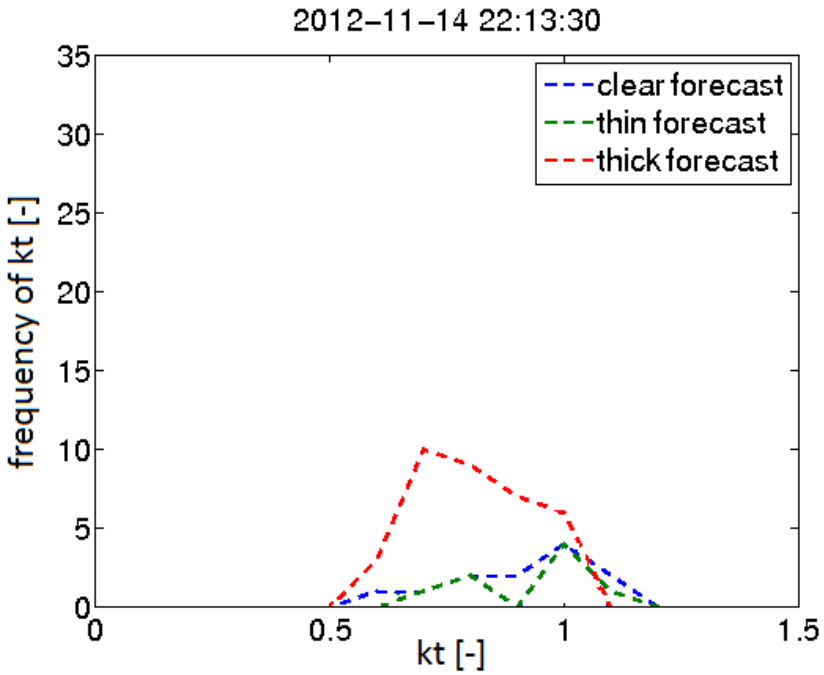

Figure 4. Histogram of kt measurements from six pyranometers within the sky imager footprint during the lookback period of 5 minutes. The peaks of each histogram represents kt_{cc}, to be forecasted for forecast horizons of 5-15 minutes (see title YYYY-MM-DD HH:MM:SS UTC) on 14th November, 2012

As shown in Fig. 4, three histograms are formed using data from the lookback period and their peaks represent the *kt* values used for GHI forecasts for forecast horizons of 5-15 minutes. The peaks from the histograms are compared with *kt* measurements from sensors (asigned to cloud classes and averaged) for 5, 10, and 15 minute forecast horizons of each cloud class in Table 1.

Table 1. kt obtained from peaks of the three histograms shown in Fig. 4 are compared to measured sensor readings at times corresponding to forecast horizons of 5, 10, and 15 minutes to analyze the performance of the histograms. There were no readings for thin clouds at fh=10 and fh=15 minutes.

Cloud class	**Forecasted *kt* from histogram**	**Measured *kt* for forecast horizons (fh) of 5, 10 and 15 min**		
		fh = 5 min	fh = 10 min	fh = 15 min
Clear sky	1.00	1.00	1.10	1.10
Thin cloud	0.99	0.92	-	-
Thick cloud	0.70	0.62	0.58	0.44

At any given time, these values are used as the *kt* for their respective cloud class to estimate GHI for all forecast horizons. For instance, in the figure, at 22:13:30 UTC, the *kt* to be forecasted for thick cloud for all forecast horizons (5-15 minutes) is 0.7. Table 1. implies that the algorithm performed extremely well for a clear sky and thin cloud. For thick cloud, a 5-minute forecast performed better than 10 and 15 minute forecasts. The measured *kt* readings were obtained from sensors and these values are not available during a real-time functioning of the USI and were obtained from data available at the end of the day.

It is interesting to note how small the difference in *kt* of clear sky (1.00) and thin cloud (0.99) is when obtained from the histogram, and also the fact that the estimated *kt* for thick clouds (0.7) has been overestimated by the algorithm. More can be understood from Fig. 5. which shows the various steps of the USI at 22:11:30 UTC on 14th November, 2012; 2 minutes before the time that is represented in the histogram in Fig. 4. Cirrus clouds (thin wispy clouds) and cirrocumulus clouds (thin clumpy clouds) are present in the image. These clouds can sometimes cause incorrect cloud decisions depending on their position and the position of the sun. Due to the effect of the sun, it is unclear whether the lower region of the circular image is a thin cloud or thick cloud. If it is a thin cloud, it would have a higher *kt* which would be assigned to a thick cloud *kt* due to cloud decision (which has detected thick cloud) and hence overestimate the thick cloud *kt*. Similarly, the reason for the algorithm having overestimated the thin cloud *kt* by 0.7 could be due to the cloud decision algorithm incorrectly assigning thin cloud to clear sky pixels towards the center of the image. Although incorrect cloud decision

can reduce accuracy of the forecast *kt* from the histogram, the cloud decision algorithm has caused major discrepancies only during rare incidents such as the presence of certain clouds such as cirrus and cirrocumulus and the position of the sun or rain drops on the sky imager during rainfall.

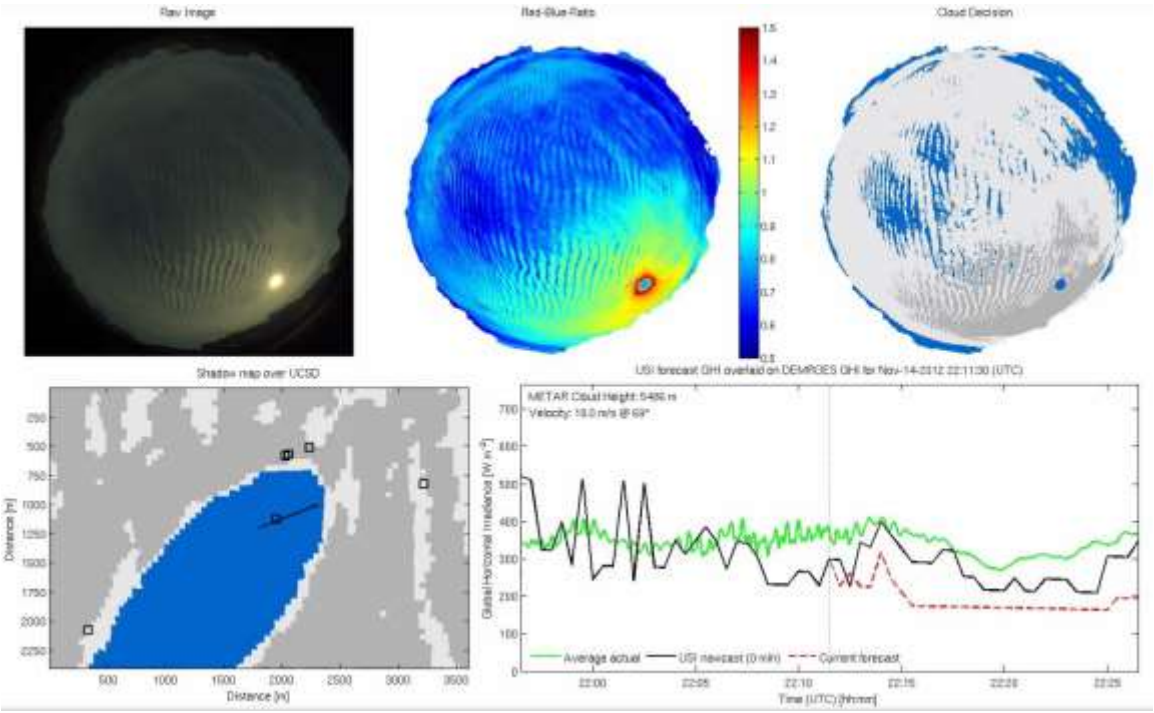

Figure 5. Steps involved in USI forecast algorithm, showing presence of Cirrus and Cirrocumulus clouds over the UCSD footprint at 22:11:30 UTC on 14th November, 2012.

Fig. 6 shows a summary plot for 14th November, 2012. The plot represents a comparison of forecasted values of *kt* for each cloud class at every timestep throughout the entire day and the *kt* measured for each cloud class (using cloud detection) by pyranometers; for a 5-minute forecast.

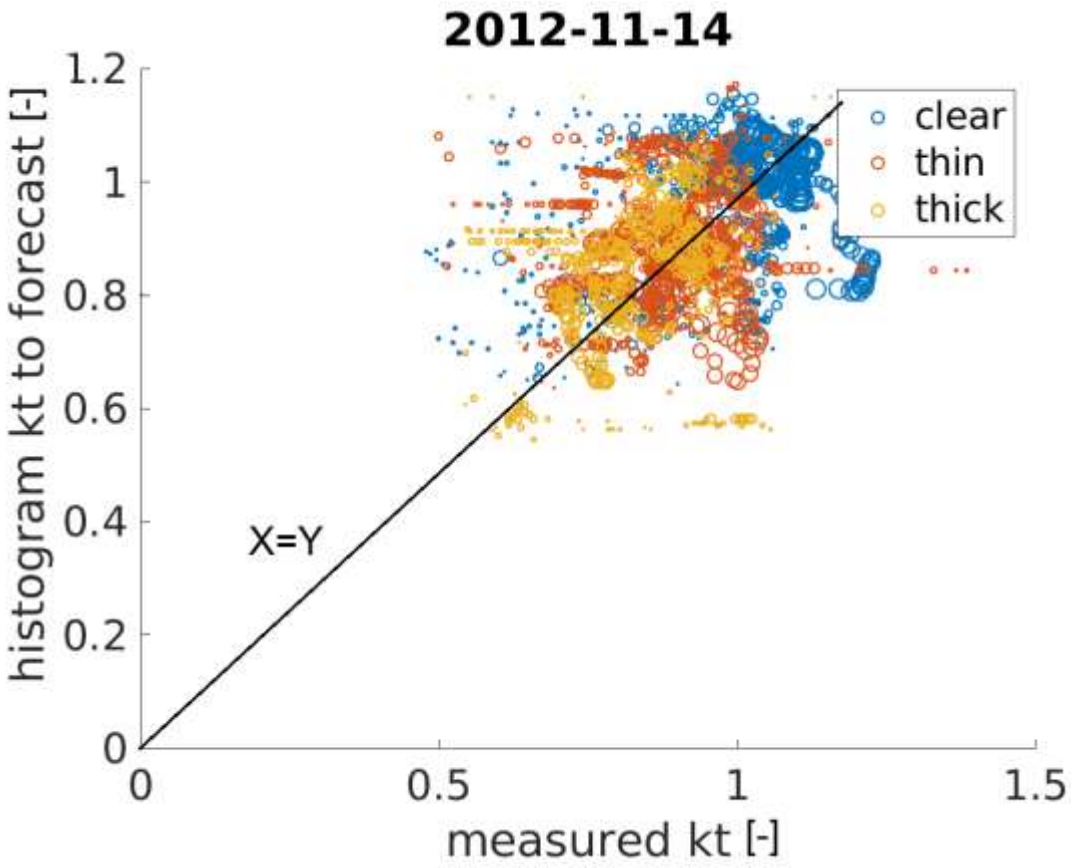

Figure 6. Plot showing data points representing kt measured by pyranometres on Y axis and kt forecasted by histograms on X axis for their respective cloud classes for the month of November, 2012.

The cluster of data points in the affinity of the $X = Y$ line indicate the successful performance of the algorithm. The overlapping of the range of *kt* of the three cloudclasses with each other indicates the advantage of this method over the existing method as stated earlier as it allows us to choose a *kt* for a cloud class without restricting it to any range. The *kt* values in the existing method would not overlap because the method restricts the value of *kt* to particular bounds which has been predefined while forming a histogram, and do not overlap with those of other cloud classes.

A way of quantifying the performance of the new algorithm was to draw an error metrics comparing the RMSE (root mean square error) and the MBE (mean bias error) for the new algorithm with that of the existing algorithm. In the following equations, N denotes the total set of forecasts generated on a given day. kt^f denotes *kt* forecasted by the histogram algorithm and kt^{obs} denotes *kt* observed by sensors for the time that we are forecasting.

$$RMSE = \sqrt{\frac{1}{N}\sum_{n=1}^{N}(kt_n^f - kt_n^{obs})^2} \quad (3)$$

$$MBE = \frac{1}{N}\sum_{n=1}^{N}(kt_n^f - kt_n^{obs}) \quad (4)$$

Comparing the new to the existing method, Fig. 7(a) shows that the average RMSE was reduced from 0.23 to 0.14, and Fig. 7(b) shows that the mean of the absolute of MBE reduced from 0.11 to 0.05. Both methods performed excellently with nearly 0 RMSE on days that had an average cloud fraction of less than 1%, such as days 4-6, 11, and 13. As there were miniscule or no changes in cloud cover, the length of the lookback period or assignment of *kt* to cloud classes were not factors in determining *kt*. 8th November produced maximum error for both methods due to rain drops on the USI in the morning (which affects cloud decision). Two overlaying layers of clouds moving in different directions negatively affected forecasts owing to the challenge in correctly calculating cloud base height, which in turn creates inaccurate shadow maps. Days 10 and 17 also had prominent periods of cloud evaporation and formation and thus produced high errors which the new algorithm was able to reduce.

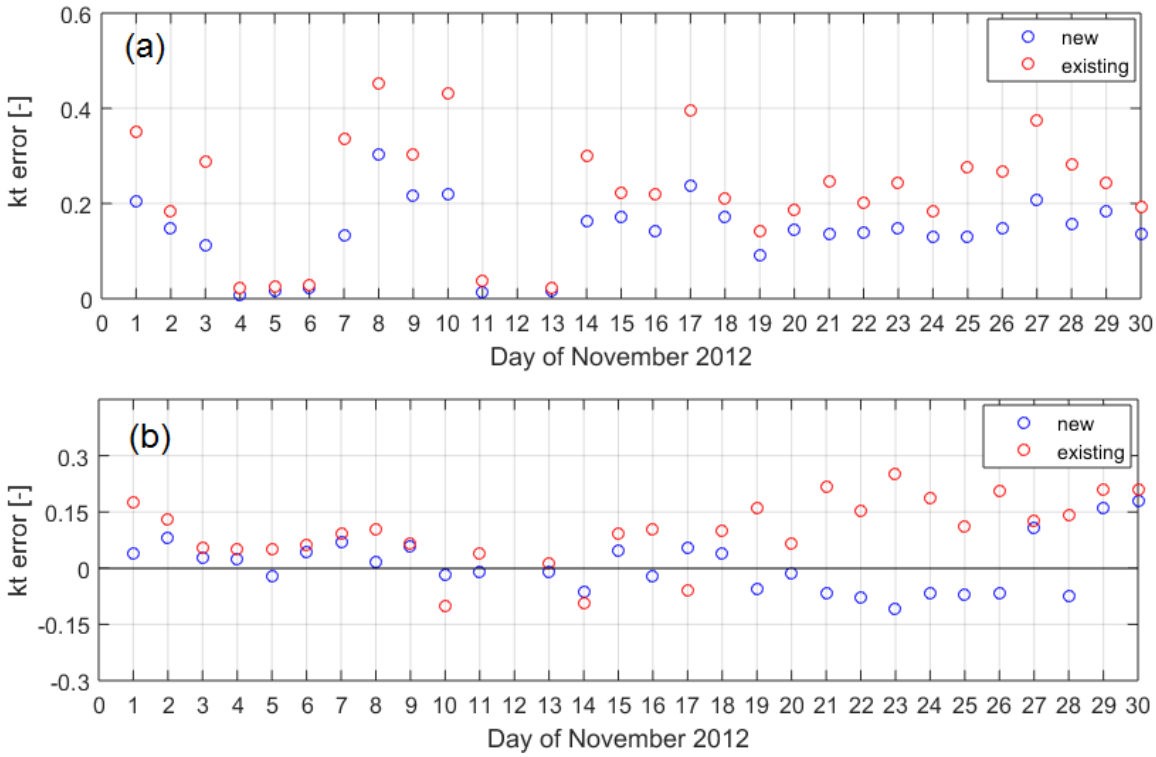

Figure 7. Error metrics of forecast kt for the new histogram algorithm and the existing algorithm, for the month of November. (a) Root mean square error (RMSE) for a 5-minute forecast kt (b) Mean bias error (MBE) for a 5-minute forecast kt.

Days 21, 23, 25 and 26 (average cloud fractions 40-50%) had multiple patches of cloud formation and dissipation, and therefore show a higher error in the existing algorithm than days 19, 20, 22 and 24 (average cloud fraction 3-15%), which had lesser instances of sudden changes in cloud cover. Days 29 and 30 (average cloud fraction 97-100%), although having overcast conditions for most of the day, had heavy rainfall, multiple cloud layers, and patches of extremely sudden cloud dissipation in the afternoon, hence increasing error. The new algorithm produced a lower RMSE on all 29 days due to better adaptation to rapidly altering cloud conditions. Yet, certain days that produced lower percentage reductions than the monthly average were due to presence of Cirrus and Cirrocumulus clouds; thin, wispy and clumpy clouds that sometimes produce incorrect cloud decision.

The MBE plot must have data as close to the 0-line to signify a good performance. As seen in the figure, MBE for the new algorithm is closer to 0 than the existing algorithm for all days. The mean MBE without considering absolute values of individual days changed from 0.10 to 0.01. While it is clearly evident from Fig. 7(b), the existing algorithm more often overestimated the *kt* while only underestimating the *kt* thrice in the entire month, and thus has a mean bias of 0.10. The new method, due to its dependency on cloud decision, displayed an unpredictable nature, which is evident from Fig. 7(b). With a mean bias of 0.01, the method overestimated *kt* on 14 days out of the 29 days while underestimating *kt* on rest of the days. November is predominantly San Diego's sunniest month and hence the existing algorithm may have performed better than it would for the rest of the year. Even better results are expected during the other months of the year due to more dynamic cloud cover.

Chapter 4 in part, is currently being prepared for submission for publication of the material. Sheth, Nishank; Murray, Keenan; Kurtz, Ben; Kleissl, Jan. The thesis author was the primary investigator and author for this material.

5. CONCLUSION

An accurate algorithm to forecast GHI quantitatively is significant for sky imagers and has remained a major challenge but the Shadow Histograms algorithm is effective to forecast GHI as inferred from the error metrics. The new algorithm highly depends on the function of cloud detection to detect cloud classes accurately. If an error occurs during the step of cloud detection, the following step of assigning *kt* to a particular cloud class gets affected. For instance, if a thick cloud over a sensor is detected as thin cloud, the *kt* measured by the sensor which should be assigned to thick cloud would be assigned to a thin cloud. Never the less, the cloud detection algorithm performs very well and seldom produces an error in detecting cloud classes accurately.

Hence, the new algorithm subsequently produces results with a lower error. Qualitatively, it produced a lower error on all 29 days of November, performing relatively better in terms of reducing error on days that experienced sudden changes in cloud cover. Quantitatively, the method gives a 39% reduction in root mean square error for November and can be estimated to give a higher reduction for other months as explained in the results. The algorithm can be applied to sky imagers using a binary cloud decision as well. The algorithm can, therefore, be added in the GHI function for the USI as well as other sky imager to calculate GHI over the footprint, and is a concrete step forward in estimating GHI with short term solar forecasting.

Chapter 5 in part, is currently being prepared for submission for publication of the material. Sheth, Nishank; Murray, Keenan; Kurtz, Ben; Kleissl, Jan. The thesis author was the primary investigator and author for this material.

REFERENCES

[1] C. W. Chow, B. Urquhart, M. Lave, A. Dominguez, J. Kleissl, J. Shields and B. Washomc, "Intra-hour forecasting with a total sky imager at the UC San Diego solar energy testbed," *Solar Energy,* pp. 2881-2893, 2011.

[2] J. Shields, M. Karr, A. Burden, R. Johnson, V. Mikuls and J. Streeter, "Research toward Multi-Site Characterization of Sky Obscuration by Clouds, Final Report for Grant N00244-07-1-009, Marine Physical Laboratory, Scripps Institution of Oceanography,University of California San Diego, Technical Note 274.," 2009.

[3] C. Gauchet, P. Blanc, B. Espinar, B. Charbonnier and D. Demengel, "Surface solar irradiance estimation with low-cost fish-eye camera," in *Remote Sensing Measurements for Renewable Energy*, Risoe, Denmark, 2012.

[4] T. Schmidt, J. Kalisch, E. Lorenz and D. Heinemann, "Evaluating the spatio-temporal performance of sky-imager-based solar irradiance analysis and forecasts," *Atmospheric Chemistry and Physics,* vol. 16, pp. 3399-3412, 2016.

[5] H. Yang, B. Kurtz, D. Nguyen, B. Urquhart, C. W. Chow, M. Ghonima and J. Kleissl, "Solar irradiance forecasting using a ground-based sky imager developed at UC San Diego," *Solar Energy,* pp. 502-524, 2014.

[6] Z. Pecenak, M. F. A, Kurtz, B., Evan, A. and J. & Kleissl, "Simulating irradiance enhancement dependence on cloud optical depth and solar zenith angle.," *Solar Energy,* vol. 136, pp. 675-681, 2016.

[7] V. Smil, "General Energetics: Energy in the Biosphere and Civilization," *Wiley,* Vols. ISBN 0-471-62905-7, p. 369, 1991.

[8] V. Smil, "Energy at the Crossroads," *Organisation for Economic Co-operation and Development,* Vols. ISBN 0-262-19492-9, 2006.

[9] S. Pelland, J. Remund, J. Kleissl, T. Oozeki and K. De Brabandere, "Photovoltaic and Solar Forecasting: Stateof the Art," *IEA:PVPS,* vol. T14, no. 1, 2013.

[10] G. Pfister, R. McKenzie, L. J.B., T. A., B. Forgan and C. Long, "Cloud coverage based on all-sky imaging and its impact on surface solar irradiance," *J. Appl. Meteorol. Climatol,* vol. 42, no. 10, pp. 1421-1434, 2003.

[11] C. Paoli, C. Voyant, M. Muselli and M.-L. Nivet, "Forecasting of preprocessed daily solar radiation time series using neural networks," *Solar Energy,* vol. 84, no. 12, pp. 2146-2160, 2010.

[12] C. Chen, S. Duan, T. Cai and B. Liu, "Online 24-h solar power forecasting based on weather type classification using artificial neural network," *Solar Energy,* vol. 85, no. 11, pp. 2856-2870, 2011.

[13] R. Marquez, P. H.T.C. and C. Coimbra, "Hybrid solar forecasting method uses satellite imaging and ground telemetry as inputs to ANNs," *Solar Energy,* vol. 92, pp. 176-188, 2013.

[14] J. Huang, M. Korolkiewicz, M. Agrawal and J. Boland, "Forecasting solar radiation on an hourly time scale using a Coupled AutoRegressive and Dynamimc System (CARDS) model," *Solar Energy,* vol. 87, pp. 136-149, 2013.

[15] R. Perez, S. Kivalov, J. Schlemmer, K. Hemker Jr., D. Renne´ and T. Hoff, "Validation of short and medium term operational solar radiation forecasts in the US," *Solar Energy,* vol. 84, no. 12, pp. 2161-2172, 2010.

[16] E. Lorenz, D. Heinemann, H. Wickramarathne, H. Beyer and S. Bofinger, "Forecast of ensemble power production by grid-connected PV systems," in *22th European PV Conference 3-9*, 2007.

[17] R. Perez, P. Ineichen, K. Moore, M. Kmiecik, C. Chain, R. George and F. Vignola, "A new operational model for satellite-derived irradiances: description and validation," *Solar Energy,* vol. 73, pp. 307-317, 2002.

[18] R. C. C. Marquez, "Intra-hour DNI forecasting based on cloud tracking image analysis," *Solar Energy,* vol. 91, pp. 327-336, 2013.

[19] B. Urquhart, C. Chow, D. Nguyen, J. Kleissl, M. Sengupta, J. Blatchford and D. Jeon, "Towards intra-hour solar forecasting using two sky imagers at a large solar power plant," *Proceedings of the American Solar Energy Society, Denver, CO, USA,* 2012.

[20] PREPA, "Puerto Rico Electric Power Authority Minumum Technical Requirements for Photovoltaic Generation (PV) Projects," 2012.

[21] B. Urquhart, B. Kurtz, E. Dahlin, M. Ghonima, J. E. Shields and J. Kleissl, "Development of a sky imaging system for short-term solar power forecasting," *Atmospheric Measurement Techniques,* pp. 875-890, 2015.

[22] J. Yang, Q. Min, W. Lu, W. Yao, Y. Ma, J. Du, T. Lu and G. Liu, "An automated cloud detection method based on the green channel of total-sky visible images," *Atmospheric Measurement Techniques,* pp. 4671-4679, 2015.

[23] J. E. Shields, M. E. Karr, R. W. Johnson and A. R. Burden, "Day/night whole sky imagers for 24-h cloud and sky assessment: history and overview," *Applied optics,* pp. 1605-1616, 2013.

[24] M. S. Ghonima, B. Urquhart, C. W. Chow, J. E. Shields, A. Cazorla and J. Kleissl, "A method for cloud detection and opacity classification based on ground based sky imagery," *Atmospheric Measurement Techniques,* pp. 2881-2892, 2012.

[25] M. S. Ghonima, "Electronic Theses and Dissertations UNIVERSITY OF CALIFORNIA , SAN DIEGO Aerosol effects on Red Blue Ratio of Clear Sky Images , and Impact on Solar Forecasting A Thesis submitted in partial satisfaction of the requirements for the degree Master of Scienc," 2011.

[26] C. N. Long, J. M. Sabburg, J. Calbo' and D. Pages, "Retrieving Cloud Characteristics from Ground-Based Daytime Color All-Sky Images," *JOURNAL OF ATMOSPHERIC AND OCEANIC TECHNOLOGY,* pp. 633-652, 2006.

[27] P. Davison, D. Roberts, R. Arnold and R. Colvile, "Estimating the direct radiative forcing due to haze from the 1997 forest fires in Indonesia," *Journal of Geophysical Research, [Atmospheres],* vol. D10207, p. 109, 2004.

[28] N. Feng and S. A. Christopher, "Clear sky direct radiative effects of aerosols over Southeast Asia based on satellite observations and radiative transfer calculations," *Remote Sensing of Environment,* vol. 152, pp. 333-344, 2014.

[29] B. Urquhart, M. Ghonima, D. Nguyen, B. Kurtz, C. Chow and J. Kleissl, "Sky imaging systems for short-term solar forecasting," in *Solar Energy Forecasting and Resource Assessment*, 2013.

[30] V. Smil, "Does Energy Efficiency Explain Japan's Economic Success?," *Current History,* vol. 90:555, p. 175, 1991.